

Article

Cs_xCo/Na-MOR Coating on Ceramic Monoliths for Co-Adsorption of Hydrocarbons Mixture and Selective Catalytic Reduction of NO_x

Ramiro M. Serra, Leticia E. Gómez, Inés S. Tiscornia, María de los Milagros Deharbe and Alicia V. Boix * 

Institute of Research in Catalysis and Petrochemistry, CONICET, Chemical Engineering School, Universidad Nacional del Litoral, Santa Fe 3000, Argentina

* Correspondence: aboix@fiq.unl.edu.ar; Tel.: +54-342-4536861

Abstract: In this work, ceramic monoliths were coated with powders based on exchanged Cs and/or Co cations in Na-mordenite (MOR) zeolite. SEM images showed that zeolite particles fill the macropores of cordierite walls and form a continuous layer of approximately 40 μm with good adherence. XPS analysis revealed that Co and Cs are present on the film surface solely as Co²⁺ and Cs⁺ at exchange positions in zeolite. The monolithic structures were evaluated for the butane-toluene co-adsorption and SCR of NO_x with hydrocarbon mixture as the reducing agent. The presence of alkali metal cations in the zeolitic lattice favored the adsorption capacity of both hydrocarbons, while cobalt cations provoked a decrease in the adsorbed amounts due to its weak interaction with the HCs. Breakthrough curves of butane adsorption showed a roll-up phenomenon, associated with a competitive adsorption effect generated from toluene presence. In the desorption process, it was observed that adsorbed toluene hindered the butane diffusion through mordenite channels, which released at higher temperatures (above 250 °C). Cs₂CoM and Cs₇CoM monoliths were more active than the CoM monolith for NO-SCR. The presence of Cs cations close to Co cations increased the hydrocarbons concentration around active sites at high temperatures, according to TPD results, promoting the reduction activity of NO.

Keywords: monolithic structures; co-adsorption; NO_x-SCR; hydrocarbons mixture; toluene-butane



Citation: Serra, R.M.; Gómez, L.E.; Tiscornia, I.S.; Deharbe, M.d.l.M.; Boix, A.V. Cs_xCo/Na-MOR Coating on Ceramic Monoliths for Co-Adsorption of Hydrocarbons Mixture and Selective Catalytic Reduction of NO_x. *Catalysts* **2023**, *13*, 106. <https://doi.org/10.3390/catal13010106>

Academic Editors: Juan Pablo Bortolozzi and Ezequiel David Banus

Received: 29 November 2022

Revised: 22 December 2022

Accepted: 28 December 2022

Published: 3 January 2023



Copyright: © 2023 by the authors. Licensee MDPI, Basel, Switzerland. This article is an open access article distributed under the terms and conditions of the Creative Commons Attribution (CC BY) license (<https://creativecommons.org/licenses/by/4.0/>).

1. Introduction

Nitrogen oxides (NO_x), unburned hydrocarbons (HCs), greenhouse gas (CO₂), and particulate matter (PM), among others, emitted from fossil fuel combustion are the major air contaminants. These pollutants cause serious environmental problems, such as photochemical smog, acid rain, global warming, and ozone layer depletion that harm human health and ecosystems.

The regulations concerning the emissions of harmful exhaust gas combustion effluents are becoming more stringent, requiring the development of highly efficient catalytic aftertreatment technologies. In the review by Zhang et al. [1], the decrease in the limit concentrations of gaseous contaminants (NO_x, HCs, CO) and particulate matter (PM) according to European Union (EU) heavy vehicle emission standard is shown.

The great efforts worldwide to reduce emissions from vehicles continue to advance to achieve reductions greater than 99.5% in the engine exhaust in order to comply with the new stricter regulations. At the same time, fuel economy regulations are being implemented in order to reduce CO₂ emissions and consequently global warming [2].

Improving the efficiency of post-treatment catalysts requires the design and development of new materials, where a major goal is to reduce NO_x and hydrocarbon emissions during the cold start conditions. In this line, a recent issue published by *Catalysts* [3] compiles the studies of various research groups concerning catalytic systems for the control

of emissions from internal combustion engines, including CO and HCs oxidation, NO_x and HCs traps, NO_x reduction, and particulate matter filtration.

Three-way catalysts (TWCs) have been successfully used on gasoline engines to simultaneously convert HCs, CO, and NO_x with high efficiency once the catalyst has achieved its minimum operating temperature (between 250 to 400 °C) after a cold start [4]. In this sense, the review by Farrauto et al. [2] summarizes the most significant technological advances of the last 40 years in catalysis for the control of emissions from internal combustion engines. The authors pointed out that as a consequence of fuel economy and fuel cut implementations, a decrease in exhaust gas temperature occurs, therefore emission control during cold start currently remains a major challenge.

The progress of diesel exhaust after-treatment technology has required the development of the diesel oxidation catalyst (DOC), selective catalytic reduction (SCR) catalyst with urea injection, and diesel particulate filter (DPF), which are active for reducing the pollutants when they have reached a minimum operating temperature. Approximately 1 to 3 min is required for the diesel emission control system to become active after a cold start [1,3,4].

To reduce the emission of pollutants into the atmosphere during the cold-start stage of the engine, different strategies have been proposed. Among them, the electrical heating of the catalytic converter or the injection of excess fuel into the combustion chamber have been attempts to quickly reach the minimum operating temperature of the catalyst. However, these proposals go against the fuel economy of the vehicle [4].

The most promising after-treatment technology is to adsorb the harmful gases at a low temperature (NO_x, hydrocarbons) in a trap and later release and convert them at a higher temperature (light-off temperature). A significant amount of research has emerged recently in the literature regarding hydrocarbon traps (HCT) and passive NO_x adsorber (PNA) [2,4]. In this vein, Lee et al. [4] describes the current trapping technologies applied in vehicle exhaust systems during the cold-start stage. One strategy is to employ a HC trap that can adsorb the HC emissions at low temperatures and then oxidize the stored HCs at higher temperatures. To reduce the NO_x emissions, a passive NO_x adsorber (PNA) can adsorb and retain NO_x during the cold start, until the selective NO_x reduction catalyst reaches an active temperature where desorption and conversion can occur.

Barbera-Italiano et al. [5] studied a system able to reduce the pollutants during the cold-start phase. The authors analyzed the adsorption efficiency of commercial microporous powders (active carbons and zeolites) at different temperature using gas compositions representative of driving conditions. The sorption capacity of materials was measured for different representative harmful gases (CO, NO_x, CO₂, toluene, pentane, acetylene, NH₃, CH₄, etc.) present in the exhaust stream.

In the literature, there are a large number of studies that examine different aspects related to the properties of adsorbent, which have to meet certain requirements for their practical application: the materials have to be able to adsorb most of the gases present without preferential selectivity towards certain compounds; in addition, the HC traps have to be resistant to potential inhibitors present in the exhaust stream. Zeolites have been widely used as support material for HC traps due to their diversity of structure, chemical composition, pore size, and versatility to incorporate different cations to improve adsorption–retention capacity [6–12].

In our previous works, we have studied the adsorption of toluene in zeolites modified with alkali metals as potential hydrocarbons traps during cold start, where the beneficial effects of Cs on the adsorption capacity and desorption temperature were investigated [13–15].

In recent decades, special attention has been paid to research concerning the abatement of nitrogen oxides in order to comply with environmental regulations. Nowadays, the selective catalytic reduction (SCR) is probably the most widespread process for limiting NO_x emissions under lean conditions (O₂ excess). The NO_x-SCR with NH₃ or urea as a reducing agent is used in stationary sources, while the three-way catalysts are employed in mobile sources. Furthermore, selective catalytic reduction using hydrocarbons has been an alternative that allows the use of a mixture of gases similar to those found in the exhaust

stream. Since the pioneering work of Iwamoto and Yahiro [16] in the 1990s, catalysts for HC-SCR using metal-exchange zeolites have been extensively developed up to now due to their tunable properties and thermal stability [17–19].

The majority of the studies related to the different processes for the abatement of harmful exhaust gases combustion effluents were performed in microreactors using powder catalysts. However, for practical applications these catalysts should be shaped in a monolithic structure [20]. There are several ways to prepare monoliths, washcoating is one of the simplest methods employed for attaching the active phases on the monolith walls. Our group studied metal-zeolites deposited on monoliths for the selective catalytic reduction of NO using methane or butane as a reducing agent. Very active and selective formulations were obtained by combining exchanged metals (Pt and Co) in the zeolitic lattice [21–24].

In recent works, different strategies have been proposed in order to couple adsorption processes and selective catalytic reductions in order to prevent the emission of polluting gases during cold start [25,26]. In this vein, in our previous work, powdered Na-mordenite exchanged with Co and/or Cs were studied for toluene or butane adsorption at low temperature. Furthermore, the selective catalytic reduction of NO_x using these hydrocarbons as reducing agents was evaluated [27].

In the present work, we extend the investigation of Cs_xCo-MOR to a more realistic application, using a honeycomb monolith structure. The challenge is that the catalytic activity achieved by Co incorporating as an active metal into the SCR, and the hydrocarbon adsorption properties improved by Cs incorporation, are preserved in the structured system. In addition, the structured systems were evaluated using a mixture of hydrocarbons (toluene-butane) analyzing the effect caused by the presence of an aromatic hydrocarbon together with a linear alkane in the stream. The monolithic samples were conveniently adapted in order to characterize them by means of XPS and SEM microscopy.

2. Results and Discussion

2.1. Physicochemical Characterizations

The compositions of the commercial zeolite and synthesized powders by ion exchange method are detailed in Table 1. Commercial Na-MOR presents 4.2 wt.% of Na concentration, the expected value for this zeolite, which decreased after subsequent exchanges. The catalyst Co/Na-MOR shows a cobalt content of 2.9 wt.%, while in bimetallic samples, the Co content is 2.5 wt.%. On the other hand, percentages of cesium incorporated are close to nominal values for all materials (2 and 7 wt.%). In addition, Mg, Ca, and K cations present in parent Na-MOR in low concentration (<wt.%) were not detected by ICP after the exchanges.

Table 1. Elemental composition of powders and monolithic samples.

Powder Composition	Na (wt.%)	Co (wt.%)	Cs (wt.%)	Monolithic Sample
Na-MOR	4.2	—	—	M
Co/Na-MOR	1.8	2.9	—	CoM
Cs ₂ /Na-MOR	3.2	—	1.9	Cs ₂ M
Cs ₇ /Na-MOR	2.7	—	7.1	Cs ₇ M
Cs ₂ -Co/Na-MOR	1.6	2.5	1.8	Cs ₂ CoM
Cs ₇ -Co/Na-MOR	1.1	2.5	7.3	Cs ₇ CoM

Structured samples were obtained by the washcoating technique from the synthesized powder catalysts and their labels are indicated in Table 1. In general, about 6–7 cycles of immersion, blowing, and drying were required to achieve 200 mg of active material deposited on each cordierite monolith.

Monolithic systems were evaluated to apply them in the hydrocarbons adsorption process, as well as in the selective catalytic reduction of NO with O₂ excess. Therefore,

mechanical stability of the coating film is an important parameter to be studied for further application under real conditions. Figure 1 shows the mass (in percentage) of different monolithic structures as a function of the number of sonication cycles for three minutes of each cycle. In general, the analyzed structures showed a similar behavior, reaching film stability after the fifth cycle. According to the figure, weight loss between 8 and 13% was obtained, indicating good adherence of the active film to the cordierite monolith for all samples. Despite the small amount of mass that was lost during the mechanical test, it was possible to confirm the stability of the active mass of all structured samples during the catalytic evaluation and the adsorption process.

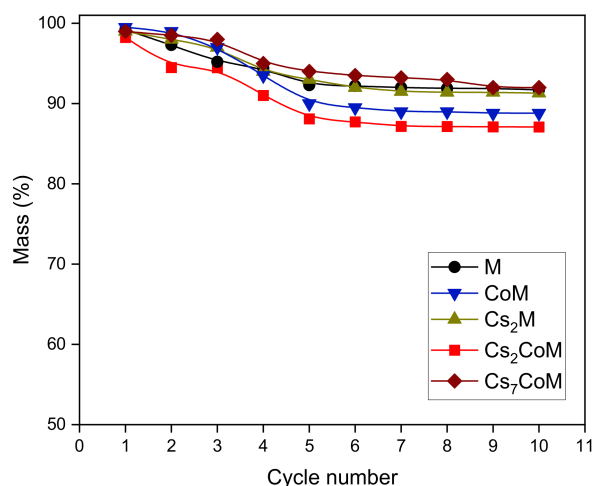


Figure 1. Mechanical stability test of active films coated on monoliths.

Figure 2 depicts optical and SEM images of the Cs₂CoM structure. The cross-section along the cordierite channels observed by optical microscope (Figure 2A) shows them covered by a continuous layer of material. On the other hand, Figure 2B shows the SEM picture of a cross-section view of a monolith, whose layer thickness is about 40 μm . In addition, some cordierite macropores filled with powder can be observed, which reveals an intimate contact between the film and the substrate favored by colloidal silica presence. Additionally, a small amount of material accumulated in the corners of monolith square cells can be detected (Figure 2C). This could have built during the blowing step of the deposition due to some fluid-dynamic phenomena. All prepared structures show similar characteristics with respect to the films obtained.

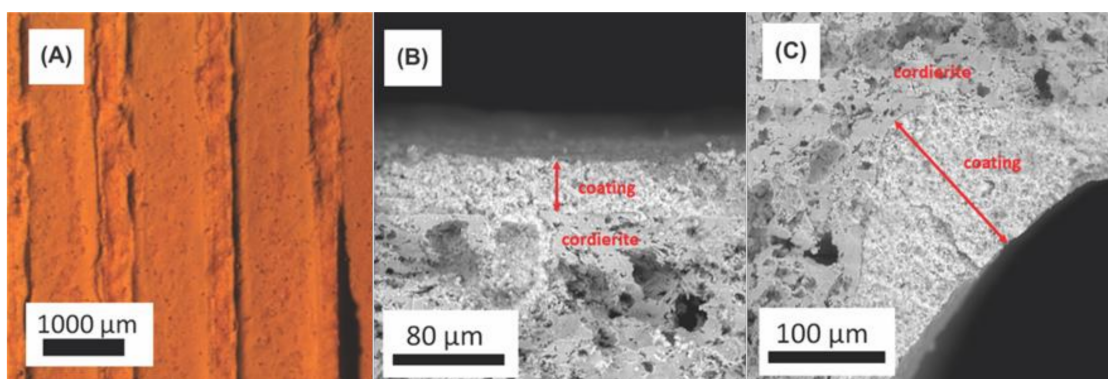


Figure 2. Images of Cs₂CoM structure: (A) optical microscopic image of a cross-section along the channels; (B) SEM image of a cross-section; (C) SEM image of corner.

X-ray diffraction results of catalytic or adsorptive structures together with those of cordierite and Na-MOR are shown in Figure 3.

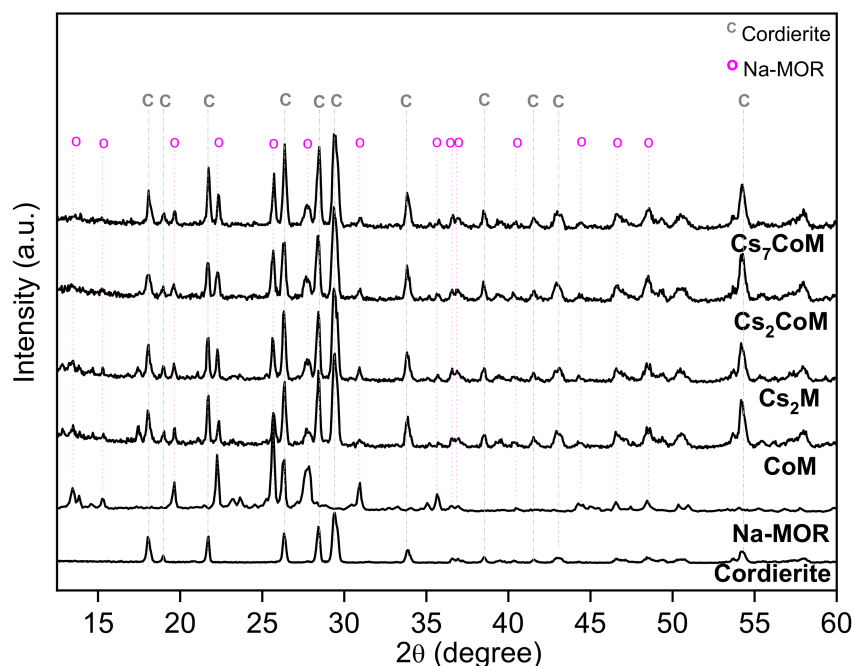


Figure 3. X-ray diffraction patterns of monolithic samples, cordierite, and Na-MOR.

The diffraction patterns of all prepared structured materials show the main peaks corresponding to the cordierite and the Na-MOR. The more intense peaks of cordierite appear at $2\theta = 18.0, 21.7, 26.3, 28.4, 29.4, 33.8,$ and 54.2 degrees, while those belong to Na-MOR appear at $2\theta = 13.4, 15.3, 19.6, 22.2, 25.6, 26.3, 27.8, 30.9, 35.6,$ and 48.4 degrees.

Although these samples contain cobalt and cesium incorporated by ion exchange, it has not been possible to detect peaks associated with these metals or metallic oxides. These results suggest that these species are present as cations, Co^{2+} and Cs^+ , in exchange positions in the zeolitic network. Moreover, signals corresponding to the main peaks of Co_3O_4 phase ($2\theta = 36.8, 31.3$ and 59.4 , JCPDS 42-1467) and Cs_2O phase (JCPDS 09-0104) are not detected, which indicates that the formation of metal oxides either did not occur or it was not possible to detect them.

A structured Cs_2CoM sample was analyzed by XPS in order to determine the elementary relative composition and oxidation state on the surface. For this purpose, a piece of the structured catalyst was placed in a special holder, and it was fixed with a niobium tape welded to the holder (Figure 4A). Before measurement, the sample was in situ treated inside the pre-treatment spectrometer chamber. It was heated at 200°C under vacuum in order to eliminate surface adsorbed molecules.

Cesium and cobalt oxidation states are identified by the deconvolution of Co 2p and Cs 3d spectra and they are showed in Figure 4B,C, respectively. Co 2p spectrum is composed by the characteristic spin-orbit splitting of Co $2p_{3/2}$ and Co $2p_{1/2}$. The Co $2p_{3/2}$ region constitutes a main signal at 782.3 eV and a satellite peak at 787.3 eV, characteristic of Co^{2+} species exchanged in zeolite lattice [28–30]. In addition, the Cs 3d spectra consists of Cs $3d_{5/2}$ and Cs $3d_{3/2}$ photoelectron peaks, whose positions are at 725.5 and 739.4 eV, respectively. These binding energy values are consistent with those reported to Cs^+ exchanged zeolite [27,31]. The calculated Cs/Co atomic surface ratio is 0.39, this value is close to that reported for bulk determination (0.32).

Raman spectra registered for powder samples Na-MOR, Co/Na-MOR, and $\text{Cs}_2\text{-Co/Na-MOR}$ are shown in Figure 5. The spectrum corresponding to the Na-MOR sample exhibits signals at $137, 191, 246, 339, 437, 494, 572,$ and 692 cm^{-1} . The Co/Na-MOR spectrum shows weaker signals at $132, 243, 330, 472, 595,$ and 690 cm^{-1} , whose positions are similar to that found in Na-MOR. According to the literature [32,33], the main signals of the Co_3O_4 species appears at $480, 525,$ and 690 cm^{-1} and they could be overlapped with the

signals corresponding to the zeolite. However, with the other mentioned characterization techniques, no evidence of Co_3O_4 species formation was detected. On the other hand, it has also been found that dispersed cobalt oxides and Co^{2+} exchanged in the matrix present a weak and broad signal around 600 cm^{-1} , which could also be coincident with the zeolite bands [34,35].

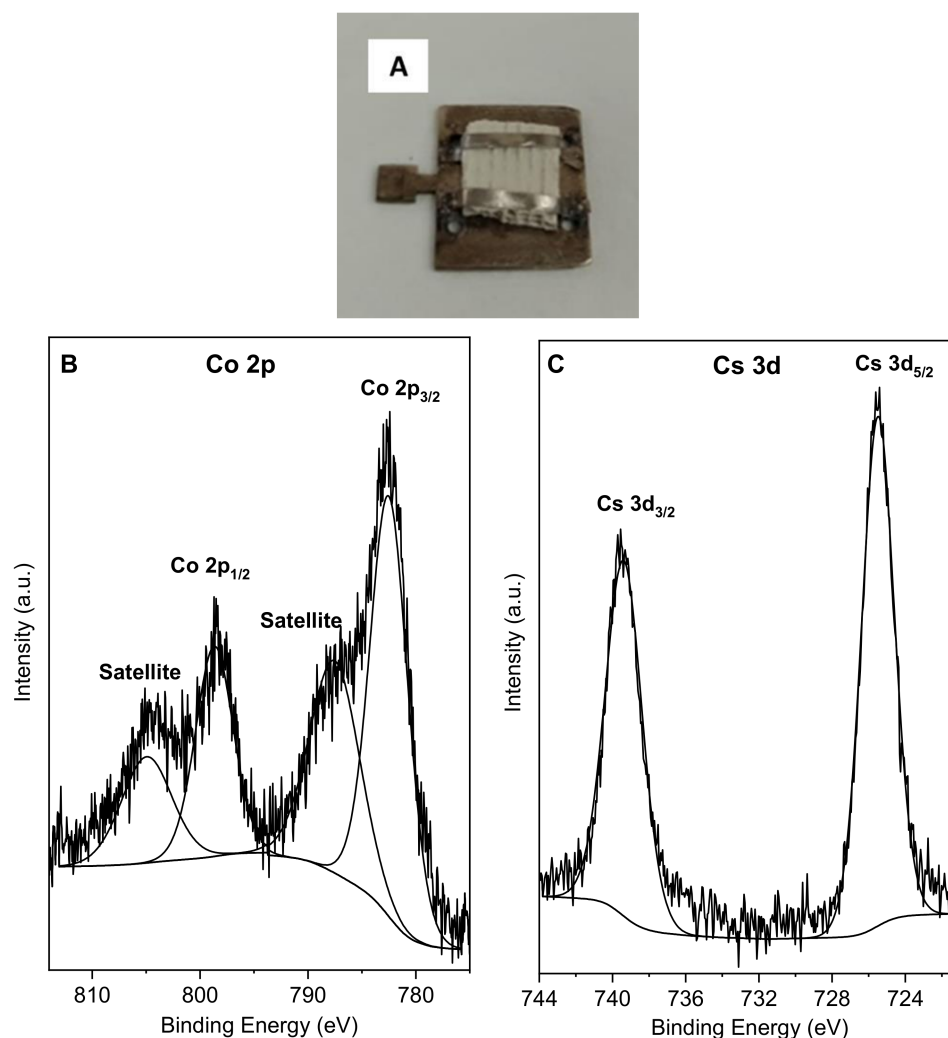


Figure 4. (A) Structured sample placed in the XPS holder. Spectra of Cs_2CoM sample: (B) Co 2p and (C) Cs 3d core levels.

The $\text{Cs}_2\text{-Co/Na-MOR}$ powder spectrum shows similar bands to Co/Na-MOR . However, no signals associated with cesium oxides could be detected [36], which also would indicate that the cesium cations are in exchange positions.

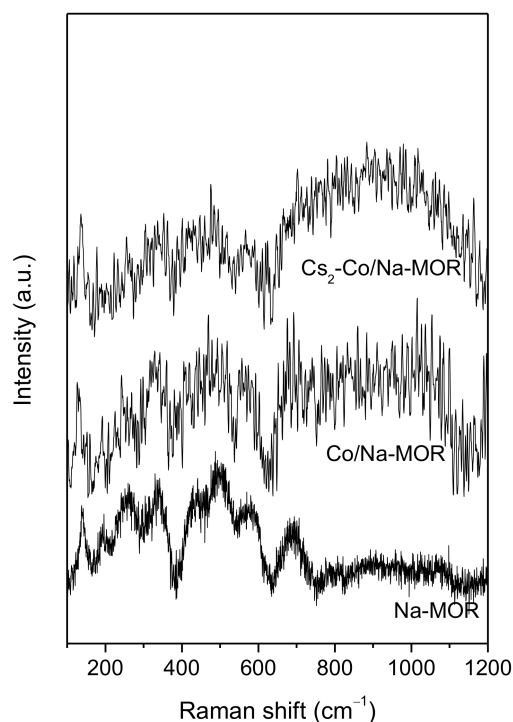


Figure 5. Laser Raman Spectroscopy (LRS) spectra of Na-MOR, Co/Na-MOR, and Cs₂-Co/Na-MOR powders.

2.2. Adsorption–Desorption Study of Toluene and Butane Mixture on Monolithic Adsorbents

Figure 6 displays the adsorption isotherms of toluene (Figure 6A) and butane (Figure 6B) obtained from the co-adsorption of both hydrocarbons on monoliths coated with exchanged mordenites, monometallic (Cs_xM or CoM), or bimetallic (Cs_xCoM). In addition, the adsorption and desorption values are listed in Table 2. The amount of hydrocarbons adsorbed at 100 °C (Q_{ads}) was determined from breakthrough curves (Figure 6).

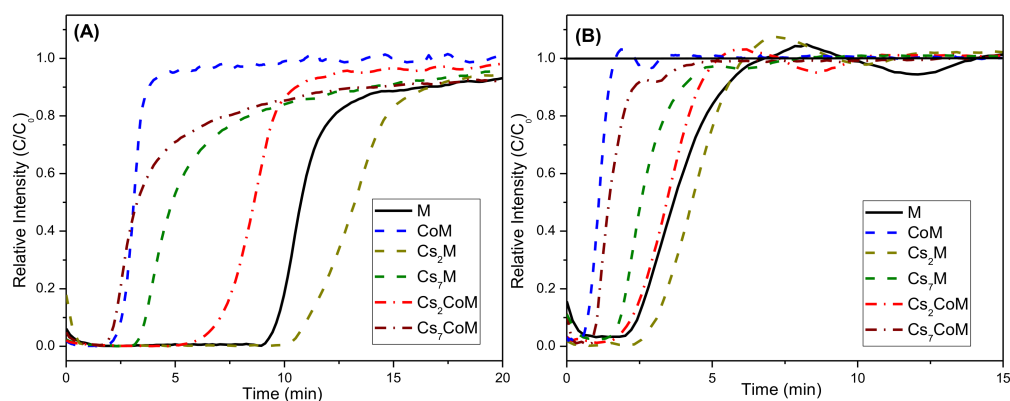


Figure 6. Breakthrough curves corresponding to the adsorption of toluene and butane mixture for M, CoM, Cs_xM and Cs_xCoM monoliths: (A) toluene; (B) butane. Conditions: T = 100 °C, 200 mg, total flow rate = 40 mL/min.

The results indicated that in all structures, the relative adsorption capacity of toluene $Q^T/(Q^T + Q^B)$ was higher than butane $Q^B/(Q^T + Q^B)$, these values were close to 83% and 17%, respectively. In the adsorption process, the chemical and physical properties of the low molecular weight linear alkane and the aromatic molecules have to be considered, among other factors [37–39]. According to several authors, the main interaction of toluene occurs between the π electrons of the aromatic ring and the Lewis sites generated (by cation

exchange), as well as between methyl groups and the zeolite framework oxygen [15,40]. On the other hand, butane only shows the interaction of C–H groups with the Lewis base center of the framework [27]. Under similar conditions, according to the breakthrough curves showed in Figure 6B, the butane reached the saturation in the adsorbent material five minutes after adsorption started. On the other hand, the saturation of toluene was reached between 5–15 min. As mentioned above, it is clear that butane was less retained due to its weaker interaction with the zeolitic structure.

Table 2. Adsorption and desorption capacities of toluene and butane mixture on monolithic adsorbents.

Monolithic Samples	^a $Q_{\text{ads}}^{\text{B}}$ ($\mu\text{mol}/\text{mg}$)	^b $Q_{\text{des}}^{\text{B}}$ ($\mu\text{mol}/\text{mg}$)	^a $Q_{\text{ads}}^{\text{T}}$ ($\mu\text{mol}/\text{mg}$)	^b $Q_{\text{des}}^{\text{T}}$ ($\mu\text{mol}/\text{mg}$)
M	0.10	0.03	0.50	0.35
CoM	0.02	0.001	0.11	0.04
Cs ₂ M	0.11	0.04	0.55	0.40
Cs ₇ M	0.07	0.01	0.35	0.25
Cs ₂ CoM	0.09	0.01	0.45	0.31
Cs ₇ CoM	0.06	0.03	0.31	0.17

^a Adsorption capacities of butane (B) or toluene (T) at 100 °C (from Figure 6). ^b Butane or toluene amount desorbed at temperatures above 100 °C (from Figure 7).

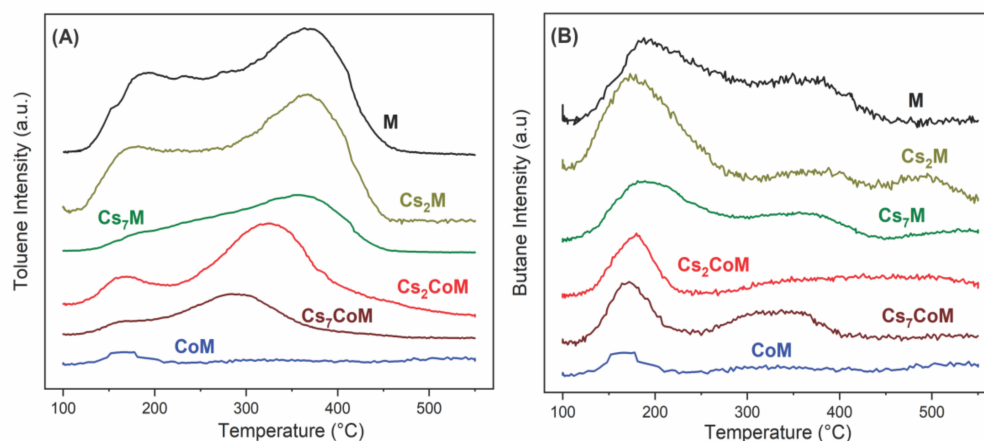


Figure 7. Profiles of temperature-programmed desorption (TPD) of (A) toluene or (B) butane after co-adsorption of butane and toluene mixture at 100 °C. Conditions: 200 mg, desorption in He flow (40 mL/min); heating rate 10 °C/min.

Regarding the M sample, commercial Na-MOR deposited on the cordierite exhibited 0.10 and 0.50 $\mu\text{mol}/\text{mg}$ of butane and toluene adsorbed, respectively. In the CoM monolith, where sodium cations were partially exchanged with cobalt, the adsorption capacity decreased about five times with respect to the M sample for both hydrocarbons. Cations with high and low electronegativity generate a change in the acid-base character of the zeolite [41,42]. In particular, the presence of cobalt cations provoked a decrease in adsorbed amounts due to weak interaction with the hydrocarbons [27]. In addition, when a low concentration of cesium (2 wt.%) was incorporated into Na-MOR (Cs₂M sample), the adsorption capacity was completely recovered and slightly overcame the adsorption values reached by the M sample. In this case, the ion-exchanged alkali cations increased the Lewis basicity, modifying again hydrocarbon adsorption properties [43]. On the other hand, a higher amount of Cs (7 wt.%, Cs₇M monolith) presented a lower adsorption capacity than M. This could be attributed to the decrease in surface area and pore volume observed in a previous study, which was related to the incorporation of bulky cesium cations in the zeolite network [14]. The presence of cobalt cations in Cs_xCoM worsened the adsorption of toluene and butane with respect to Cs_xM, due to lower sodium concentrations. It is

clear that a higher concentration of alkali metal cations in the zeolitic lattice enhanced the adsorption capacity of both hydrocarbons.

The breakthrough curves corresponding to butane adsorption (Figure 6B) show a waving shape after saturation is reached. This behavior is called a roll-up phenomenon and is observed in adsorption processes where a weakly adsorbed hydrocarbon is displaced during a competitive adsorption process by another strongly adsorbed compound [44]. In this case, toluene caused a displacement of butane, generating a competition effect until a balance of the two components was achieved.

Figure 7A,B displays TP desorption curves of toluene and butane, obtained after the hydrocarbons co-adsorption. They were performed on the structured materials and the quantified results were summarized in Table 2.

The desorption profiles of toluene are shown in Figure 7A. The M and Cs₂M monolithic samples, with the best toluene and butane adsorption capacity, present two well-defined peaks, one at low temperature, whose maximum is at 180 °C, while the other largest peak is centered at 365 °C. Likewise, bimetallic samples display two desorption peaks, but at slightly lower temperatures than the previous ones; that is, at 163 and 325 °C for Cs₂CoM and at 160 and 300 °C for Cs₇CoM. Then, monometallic Cs₇M shows a broad signal at 362 °C and another weaker one at 172 °C, while CoM exhibits only a weak signal at 164 °C.

On the other hand, butane desorption curves are displayed in Figure 7B. In general, all samples show a more intense peak between 120 and 250 °C. Additionally, M, monometallic Cs₂M and Cs₇M samples, and bimetallic Cs₇CoM present a broad signal in the medium-temperature desorption range (between 250–450 °C). In addition, another weak signal centered at 475 °C is exhibited in the Cs₂M profile, while in Cs₂CoM a broad and low-intensity peak is extended between 230 and 500 °C. The increased desorption temperature observed in the toluene profiles are expected due to the more energetically favorable adsorption of toluene in comparison with butane in all monolithic materials. As it was previously mentioned, toluene has two adsorption modes on zeolites, while the butane is adsorbed in the adsorbent by only one site.

In previous works, Serra et al. performed TPD experiments on butane and toluene individually adsorbed on powder mordenite adsorbents modified with Co and/or Cs [14,27]. In general terms, two desorption peaks were determined in the TPD curves of toluene, in a temperature range of 100–500 °C, while for butane desorption a unique peak was observed between 100 and 250 °C. This behavior revealed in each experiment was correlated to the adsorption zones of toluene and butane, respectively.

In the present work, where butane and toluene were simultaneously adsorbed, the desorption curves show that in the most materials the butane desorption continues beyond 250 °C, even up to 500 °C. This phenomenon is compatible with the single-file diffusion mechanism proposed by Czaplewski et al. [45]. They suggested that in a process where two hydrocarbons were adsorbed on a pseudo unidimensional zeolite (H-Mordenite) at the same time, the hydrocarbon with the lower diffusion coefficient acted as a plug to the other hydrocarbon, thus retarding the desorption of the lightest one [46,47]. In this case, toluene, due to the higher size, acted as plug and trap to butane avoiding its diffusion through the main channel of the mordenite and it is released at higher temperature, in the desorption experiment.

Figure 8 shows the retention capacity of butane and toluene reached by the CoM sample and bimetallic materials Cs₂CoM and Cs₇CoM. The retention capacity parameter is calculated as the desorbed and adsorbed hydrocarbon quantity ratio, $(Q_{\text{desorbed}}/Q_{\text{adsorbed}}) \times 100$, where this parameter represents the ratio between the retention capacity above 100 °C (in the range of the experiment), with respect to the total amount of adsorbed hydrocarbon. This analysis was performed over cobalt-content materials due to the cobalt species constituting the active site for the SCR-NO_x.

In the case of CoM, 36% of toluene and only 5% of butane were retained at temperatures above to 100 °C. However, the addition of 2 wt.% of cesium to CoM increased the retention capacity, reaching 69% and 13% for toluene and butane hydrocarbons, respectively. When 7 wt.% of cesium was added to CoM, the retention capacity was 55% in the case of toluene,

which was somewhat less than the increase generated by 2 wt.% of Cs due to the appearance of other factors that influence the adsorption–desorption process, as textural properties of solids. In the case of butane, the retention capacity was 48.3%.

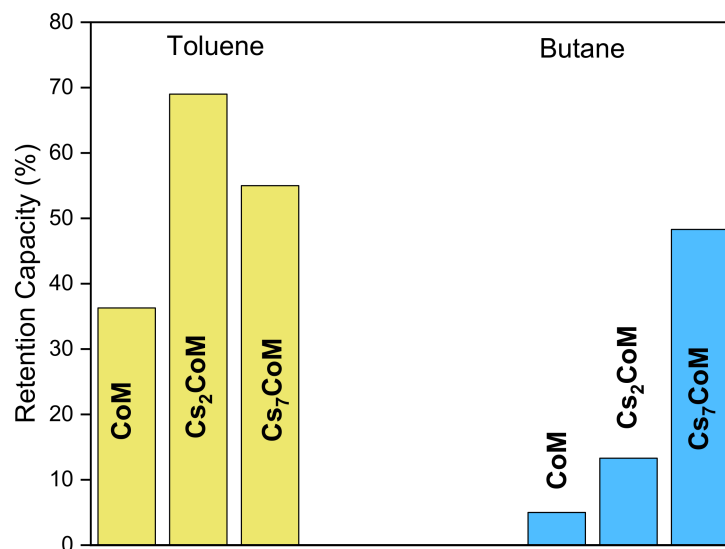


Figure 8. Toluene and butane retention capacity for hydrocarbon mixture adsorption on monolithic CoM and Cs_xCoM adsorbents.

In general, for this study, the Cs addition to CoM improved the retention capacity of toluene and butane hydrocarbons. Compared to CoM, the Cs₂CoM increased the butane retention capacity by 2.6 times, and almost doubled the toluene one. Although the addition of 7 wt.% of Cs to CoM raised the retention capacity, it was lesser than that achieved by the Cs₂CoM for the toluene. This fact could be related to the steric problems, where an increment of a voluminous cation as Cs⁺ hinders the adsorption and desorption of a molecule of a size as large as the toluene. On the other hand, for butane, an increase in cesium concentration increased the retention capacity.

2.3. Selective Catalytic Reduction of NO_x Using Toluene and Butane Mixture in the Presence of O₂ Excess

Figure 9 shows the NO to N₂ conversion in the SCR reaction as a function of temperature over the CoM, Cs₂CoM, and Cs₇CoM monolithic catalysts. A mixture of C₄H₁₀–C₇H₈ was used as reductant agent in presence of O₂ in excess. The bimetallic Cs_xCoM structures were the most active catalysts, reaching about 80% of NO conversion at 450 °C. On the other hand, monometallic CoM reached a maximum conversion of 65% at the same temperature. Above this temperature, the three NO conversion curves showed a decrease. That is, at temperatures higher than 450 °C, the hydrocarbon combustion side reaction was favored, leading to a drop in NO conversion in that temperature region. The presence of cobalt and cesium cations inside of the mordenite network improved the NO to N₂ conversion, compared to the monometallic cobalt sample, when the temperature overcomes 375 °C.

On the other hand, the hydrocarbon conversions were also analyzed. For the three catalysts, the conversion increased as the temperature raised, reaching total conversion in the 400–450 °C range, with the typical HCs oxidation performance [48,49].

It is well known that the cobalt species, mainly Co²⁺ ions exchanged in the zeolite, are the active sites for the selective catalytic reduction of NO with hydrocarbons. Nevertheless, the introduction of cobalt could also result in a variety of species, the mentioned Co²⁺ lattice cations, Co-oxo cations, and oxide-like Co species [18,50,51]. Lim and coworkers [52] concluded that the location and type of cobalt ions could differ according to the structure type and composition of the zeolite and therefore in the SCR activity when methane was employed as a reductant. In this sense, Aspromonte et al. reported a detailed study of

the nature of cobalt species of cobalt-based catalysts prepared with ZSM5, MOR, and BEA zeolites and using butane or toluene as reducing agents [53]. The authors identified Co_3O_4 , Co_xO_y , and Co^{2+} ions located at exchange positions in the calcined Co-zeolites. On the other hand, Boix et al. [24] studied the NO_x -SCR with hydrocarbons (butane or methane) on cordierite monoliths coated with Co-mordenite. Different characterizations performed on Co-mordenite catalysts revealed again the Co^{2+} ion exchanged as the main Co species present in the more selective catalysts. In particular, when a monolith prepared with 3 wt.% of cobalt was tested with butane as the reducing agent, a maximum of 53% of NO to N_2 conversion was achieved, in a temperature interval between 400–425 °C.

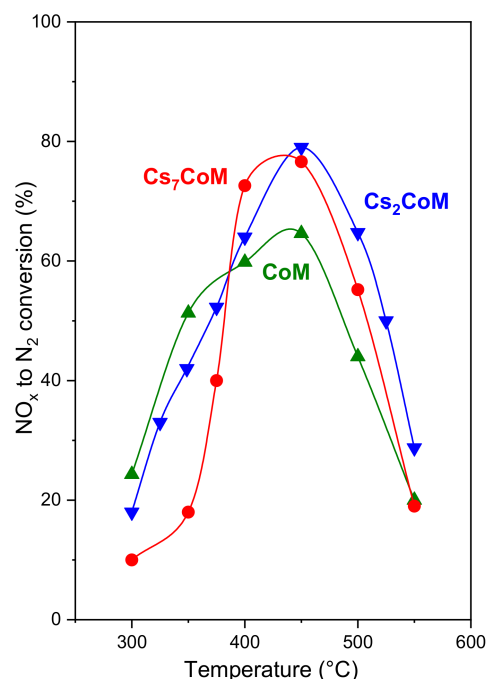


Figure 9. NO_x -SCR by C_4H_{10} - C_7H_8 mixture over CoM (\blacktriangle), Cs_2CoM (\blacktriangledown), Cs_7CoM (\bullet). Reaction conditions: 1000 ppm NO, 250 ppm toluene, 500 ppm butane and 2 vol.% O_2 , He balance and total flow 133 mL/min.

With regard to alkali metal cation, it was confirmed in previous work that monometallic samples constituting Cs- or Na-zeolite were not catalytic active for SCR-NO with hydrocarbons. Serra and coworkers [27] observed that the addition of different contents of cesium (2 and 7 wt.%) to the CoMordenite powder catalysts slightly affected the NO to N_2 conversion obtained with the monometallic sample, using butane or toluene as the reducing agents. The maximum NO to N_2 conversion reached by CoMordenite powder was 51% at 400 °C using butane as reducing agent, and 67% at 550 °C with toluene, where C/N ratio was equal to 2 in both cases ($W/F = 1.5 \text{ mg min/mL}$, $\text{GHSV} = 20,000 \text{ h}^{-1}$).

In our case, using butane–toluene mixture, the NO to N_2 conversion overcame 75% at 450 °C for monolithic Cs_xCoM catalysts, using $C/N = 3.75$ ($W/F = 1.5 \text{ mg min/mL}$), which would promote the NO_x conversion.

On other hand, Cs_2CoM and Cs_7CoM were more active than CoM for SCR of NO. This behavior could be associated with several factors. It is known that Co^{2+} ions are the more active species for this reaction and despite the fact that the bimetallic samples have a lower cobalt content (2.5 wt.%) they were more active than the monometallic one (2.9 wt.%). In this case, the presence of Cs cations close to Co cations increased the hydrocarbons concentration around active sites at high temperature, according to TPD results. These facts could promote the reduction activity of NO.

The bimetallic monoliths, where alkali metal Cs, promoter of HC adsorption, and cobalt, active center for the SCR, were combined in the zeolite, proved to be good adsorbents of hydrocarbons at low temperatures and later catalytically active.

3. Materials and Methods

3.1. Powder Preparation

The samples were prepared according to a previously studied method [27]. Na-MOR zeolite (Si/Al = 6.5, Zeolyst CBV-10 A) was chosen as support to incorporate cobalt and/or cesium species. The ionic exchange technique was applied to obtain the powder samples; Co/Na-MOR with 2.9 wt.% of cobalt was prepared from a cobalt acetate solution (0.05 M) in contact with the Na-MOR commercial zeolite. Cs_x/Na-MOR was performed by using a cesium acetate solution (1.10⁻⁵ and 0.005 M), obtaining materials with 2 and 7 wt.% of cesium (x subscript), respectively. Bimetallic Cs_x-Co/Na-MOR materials were prepared by consecutive ion-exchange processes, where the cobalt was incorporated in first place. Then, cesium was added by a second ionic exchange process over Co/Na-MOR, which was put in contact with the cesium solution. Ionic exchange processes were carried out by stirring the mixture for 24 h at 60 °C. The products were recovered by filtration, washed with distilled water, and then dried in an oven at 100 °C for 8 h. Finally, the powders materials were calcined in air flow for 6 h at 500 °C.

3.2. Monolithic Structures Preparation

Structured adsorbent catalysts were prepared by using pieces of honeycomb cordierite monolith (Corning, 400 cpi, composition 2MgO-5SiO₂-2Al₂O₃) of 1 cm × 1 cm frontal area and 2 cm length as substrate. The solids were deposited onto cordierite inner walls by the washcoating technique (external walls were covered). Monoliths were immersed in 25 mL of aqueous slurry of 20 wt.% of solid concentration. Additionally, 1 wt.% of colloidal silica was added to the slurry to improve adherence. After each immersion, the structures were blown with air in order to remove the slurry excess and then dried at 100 °C for 90 min. This immersion-blowing-drying cycle was repeated as many times as necessary to achieve the desired powder loading (200 mg). Then, the samples were calcined at 550 °C during 8 h in air flow. The monolithic samples obtained were denoted as M, CoM, Cs_xM, and Cs_xCoM, where M refers to Na-MOR deposited on cordierite substrate (Table 1).

3.3. Adsorption and Temperature-Programmed Desorption of Mixture Toluene-Butane

The hydrocarbon adsorption–desorption measurements were carried out in a continuous flow system equipped with mass spectrometer. The structured sample was placed in a quartz tube reactor (inner diameter of 16 mm) inside a tubular furnace. The free space between external monolith walls and internal lateral of the quartz tube was filled with inert SiC particles to avoid bypass flow.

The prepared structure was treated in He flow, heating up to 500 °C for 6 h. Subsequently, the sample was cooled to 100 °C and it was exposed to a mixture of butane-toluene flow in He to reach saturation state. Then, a purge under He flow at 100 °C for about 30 min was carried out. TPD experiments were performed with a 10 °C/min ramp up to 550 °C. The gas mixture stream comprised 5000 ppm butane and 8000 ppm toluene balanced with He, using a total flow of 40 mL/min. The toluene concentration was achieved by passing pure He through two saturators with liquid toluene [14]. The effluent gases were monitored by quadrupole mass spectrometer (Thermostar GSD 300T Prisma Baltzers, Pfeiffer Vacuum GmbH, Nashua, NH, USA), where signals of toluene (m/e = 91) and butane (m/e = 43) were registered.

3.4. Catalytic Evaluation on Selective Catalytic Reduction of NO_x

The catalytic activity of the structured samples was tested in a fixed-bed flow reactor at atmospheric pressure. The reaction gases consisted of 1000 ppm NO, 250 ppm of toluene, 500 ppm of butane and 2 vol.% O₂, He balance and total flow 133 mL/min. The catalyst

weight/total gas flow ratio (W/F) was 1.5 mg min/mL. The temperature range studied was between 300 and 550 °C. The compounds concentrations of reactive and products gases were determined by gas chromatography (Shimadzu GC-2014, Kyoto, Japan) with a thermal conductivity detector (TCD). Zeolite 5A, Bentona-34 and Porapak Q molecular sieve columns were used to determinate N₂ and O₂, toluene and butane, respectively.

3.5. Physicochemical Characterizations

The chemical composition of powders was measured by Inductively Coupled Plasma atomic emission spectroscopy technique (ICP-AES) using a Perkin Elmer Optima 2100DV ICP-OES instrument (Waltham, MA, USA).

The mechanical stability of the washcoated active layers deposited on monoliths was evaluated in terms of their adherences to ultrasonic cavitation [54]. The prepared structures were immersed in water inside a vessel, in an ultrasonic bath for 3 min. After that, the sample was dried, and the weight was registered. Ten sequences of sonication-drying-weight registering were performed in order to evaluate the mechanical stability of the deposited layer. The retained mass (%) was calculated from the total mass of the catalytic structure.

With the objective of studying the incorporated film, different sections of the monolithic structure were examined with optical and scanning electron microscopes (SEM). The images were collected with a Leica S8 APO (Wetzlar, Germany) optical microscope equipped with a Leica LC3 digital camera (Wetzlar, Germany) and a Phenom ProX SEM operated at 15 kV.

Powders and monolithic structures diffractograms were measured on an Empyrean Panalytical diffractometer (Malvern Panalytical Ltd., Malvern, UK), with Cu K α ($\lambda = 1.542 \text{ \AA}$) radiation, operating at 40 kV and 45 mA. The measured range was $2\theta = 10$ to 60 degrees and a scan speed of 1°/min. Data processing was performed employing the X'Pert Highscore program (Malvern Panalytical).

XPS measurements were performed in a multi-technique system (SPECS), equipped with a monochromatic Al K α source and a hemispherical PHOIBOS 150 analyzer operating in the fixed analyzer transmission (FAT) mode (SPECS, Berlin, Germany). The Al source was operated at 300 W, with a pass energy of 14 kV. The working pressure in the analyzing chamber was less than 5.9×10^{-7} Pa. The XPS analyses were performed on the calcined Cs₂CoM catalyst. Before the measurement, the sample was heated up in vacuum at 200 °C in the reaction chamber of the spectrometer. The spectral regions corresponding to Co 2p, Cs 3d, O 1s, Al 2s, Si 2p, Mg 2s, and C 1s (reference B.E. 284.6 eV) core levels were recorded. The data treatment was performed with the Casa XPS program (Casa Software Ltd., Teignmouth, Davon, UK). Peaks were considered to be a mixture of Gaussian and Lorentzian functions at a 70/30 ratio.

The Raman spectra were registered using a LabRam spectrometer (Horiba-Jobin-Yvon, Edison, NJ, USA). The excitation wavelength was the 532 nm line (Spectra-Physics, Santa Clara, CA, USA) diode pump solid-state laser. The laser power was fixed at 30 mW.

4. Conclusions

Cs_x-Co/Na-MOR coatings on honeycomb monolith structures were obtained by washcoating of Co- and/or Cs-exchanged mordenite powder after 6–7 cycles of immersion-blowing-drying. It could be observed by SEM that the zeolite particles filled the macropores of the cordierite walls and formed a continuous layer of approximately 40 μm with good adherence.

The Co and Cs species exchanged in the parent Na-MOR were not modified after washcoating into the cordierite substrate, by means of XRD measurements only signals belonging to Na-MOR and cordierite were detected. XPS analysis revealed that Co²⁺ and Cs⁺ at exchange positions within the zeolitic lattice are present on the film surface.

By combining Co²⁺ and Cs⁺ cations in the same zeolitic structure, an efficient material was obtained to adsorb a hydrocarbon mixture at low temperature and retain them until a medium temperature where the SCR of NO_x begins to occur. The Cs_xCoM monolithic catalysts reached a maximum NO to N₂ conversion of 80% at 450 °C, higher than that obtained

with CoM, using a butane–toluene mixture as the reducing agent. The incorporation of Cs_xCo-mordenite on the monolithic structure significantly improved NO to N₂ conversion obtained by the previously studied powder catalysts. Although cesium species are not catalytically active, it is possible that the presence of Cs cations close to Co cations increase the hydrocarbons concentration around active sites, increasing the reducing activity of NO.

Author Contributions: Conceptualization, R.M.S. and A.V.B.; methodology, R.M.S., M.d.I.M.D., I.S.T. and L.E.G.; investigation, R.M.S., I.S.T., L.E.G., M.d.I.M.D. and A.V.B.; visualization, R.M.S., I.S.T. and L.E.G.; writing—original draft preparation, R.M.S., I.S.T. and L.E.G.; writing—review and editing, I.S.T., L.E.G. and A.V.B.; project administration, A.V.B. and R.M.S.; funding acquisition, A.B. and R.M.S. All authors have read and agreed to the published version of the manuscript.

Funding: The authors thank the financial support received from Agencia Nacional de Promoción de la Investigación, el Desarrollo Tecnológico y la Innovación (Agencia I+D+i, grant PICT 2019-1942) and Universidad Nacional del Litoral (UNL, CAI+D 2020).

Data Availability Statement: Data are contained within the article.

Acknowledgments: The authors wish to acknowledge the financial support received from the Universidad Nacional del Litoral (UNL), Agencia Nacional de Promoción de la Investigación, el Desarrollo Tecnológico y la Innovación (Agencia I+D+i) and Consejo Nacional de Investigaciones Científicas y Técnicas (CONICET).

Conflicts of Interest: The authors declare no conflict of interest.

References

1. Zhang, Z.; Tian, J.; Li, J.; Cao, C.; Wang, S.; Lv, J.; Zheng, W.; Tan, D. The Development of Diesel Oxidation Catalysts and the Effect of Sulfur Dioxide on Catalysts of Metal-Based Diesel Oxidation Catalysts: A Review. *Fuel Process. Technol.* **2022**, *233*, 107317. [[CrossRef](#)]
2. Farrauto, R.J.; Deeba, M.; Alerasool, S. Gasoline Automobile Catalysis and Its Historical Journey to Cleaner Air. *Nat. Catal.* **2019**, *2*, 603–613. [[CrossRef](#)]
3. Doronkin, D.E.; Casapu, M. Present Challenges in Catalytic Emission Control for Internal Combustion Engines. *Catalysts* **2021**, *11*, 1019. [[CrossRef](#)]
4. Lee, J.; Theis, J.R.; Kyriakidou, E.A. Vehicle Emissions Trapping Materials: Successes, Challenges, and the Path Forward. *Appl. Catal. B Environ.* **2019**, *243*, 397–414. [[CrossRef](#)]
5. Barbera-Italiano, K.; Jeudy, E.; Lecompte, M.; Laigle, E.; Norsic, C.; Chaillou, C.; Bourhis, G. Trap Efficiency of Exhaust Gas Pollutants in Microporous Sorbents under Representative Driving Conditions. *Appl. Catal. B Environ.* **2022**, *304*, 120962. [[CrossRef](#)]
6. Westermann, A.; Azambre, B.; Fiqueneisel, G.; Da Costa, P.; Can, F. Evolution of Unburnt Hydrocarbons under “Cold-Start” Conditions from Adsorption/Desorption to Conversion: On the Screening of Zeolitic Materials. *Appl. Catal. B Environ.* **2014**, *158–159*, 48–59. [[CrossRef](#)]
7. Zelinsky, R.P.; Dean, D.P.; Breckner, C.J.; Marino, S.; Miller, J.T.; Epling, W.S. Pd/BEA Hydrocarbon Traps: Effect of Hydrothermal Aging on Trapping Properties and Pd Speciation. *Appl. Catal. B Environ.* **2023**, *320*, 121938. [[CrossRef](#)]
8. Ryu, T.; Jeong, J.; Byun, S.W.; Kweon, S.; Park, J.; Bae, W.B.; Kim, D.Y.; Kim, Y.J.; Park, M.B.; Kang, S.B. Ethylene Trapping of Palladium-Impregnated Zeolites for Cold-Start Emission Control. *Chem. Eng. J.* **2022**, *442*, 136197. [[CrossRef](#)]
9. Kim, J.; Jang, E.; Jeong, Y.; Baik, H.; Cho, S.J.; Kang, C.Y.; Kim, C.H.; Choi, J. A Cu-Impregnated ZSM-5 Zeolite for Active Cold Start Hydrocarbon Removal: Cation-Type-Dependent Cu Species and Their Synergetic HC Adsorption/Oxidation Functions. *Chem. Eng. J.* **2022**, *430*, 132552. [[CrossRef](#)]
10. Lee, J.; Giewont, K.; Chen, J.; Liu, C.-H.; Walker, E.A.; Kyriakidou, E.A. Ag/ZSM-5 Traps for C₂H₄ and C₇H₈ Adsorption under Cold-Start Conditions. *Microporous Mesoporous Mater.* **2021**, *327*, 111428. [[CrossRef](#)]
11. Westermann, A.; Azambre, B.; Chebbi, M.; Koch, A. Modification of Y Faujasite Zeolites for the Trapping and Elimination of a Propene-Toluene-Decane Mixture in the Context of Cold-Start. *Microporous Mesoporous Mater.* **2016**, *230*, 76–88. [[CrossRef](#)]
12. Azambre, B.; Westermann, A.; Fiqueneisel, G.; Can, F.; Comparot, J.D. Adsorption and Desorption of a Model Hydrocarbon Mixture over HY Zeolite under Dry and Wet Conditions. *J. Phys. Chem. C* **2015**, *119*, 315–331. [[CrossRef](#)]
13. Serra, R.M.; Miró, E.E.; Boix, A.V. FTIR Study of Toluene Adsorption on Cs-Exchanged Mordenites. *Microporous Mesoporous Mater.* **2010**, *127*, 182–189. [[CrossRef](#)]
14. Serra, R.M.; Miró, E.E.; Sapag, M.K.; Boix, A.V. Adsorption and Diffusion of Toluene on Na and Cs Mordenites for Hydrocarbon Traps. *Microporous Mesoporous Mater.* **2011**, *138*, 102–109. [[CrossRef](#)]
15. Serra, R.M.; Miró, E.E.; Bolcatto, P.; Boix, A.V. Experimental and Theoretical Studies about the Adsorption of Toluene on ZSM5 and Mordenite Zeolites Modified with Cs. *Microporous Mesoporous Mater.* **2012**, *147*, 17–29. [[CrossRef](#)]
16. Iwamoto, M.; Yahiro, H. Novel Catalytic Decomposition and Reduction of NO. *Catal. Today* **1994**, *22*, 5–18. [[CrossRef](#)]

17. Mrad, R.; Aissat, A.; Cousin, R.; Courcot, D.; Siffert, S. Catalysts for NO_x Selective Catalytic Reduction by Hydrocarbons (HC-SCR). *Appl. Catal. A Gen.* **2015**, *504*, 542–548. [[CrossRef](#)]
18. Charrad, R.; Solt, H.E.; Domján, A.; Ayari, F.; Mhamdi, M.; Valyon, J.; Lónyi, F. Selective Catalytic Reduction of NO by Methane over Co,H-SSZ-13 Catalysts: Types and Catalytic Functions of Active Co Sites. *J. Catal.* **2020**, *385*, 87–102. [[CrossRef](#)]
19. Aspromonte, S.G.; Miró, E.E.; Boix, A.V. Effect of Ag–Co Interactions in the Mordenite on the NO_x SCR with Butane and Toluene. *Catal. Commun.* **2012**, *28*, 105–110. [[CrossRef](#)]
20. Rokicińska, A.; Drozdek, M.; Bogdan, E.; Węgrzynowicz, A.; Michorczyk, P.; Kuśtrowski, P. Combustion of Toluene over Cobalt-Modified MFI Zeolite Dispersed on Monolith Produced Using 3D Printing Technique. *Catal. Today* **2021**, *375*, 369–376. [[CrossRef](#)]
21. Boix, A.V.; Zamaro, J.M.; Lombardo, E.A.; Miró, E.E. The Beneficial Effect of Silica on the Activity and Thermal Stability of PtCoFerrierite-Washcoated Cordierite Monoliths for the SCR of NO_x with CH₄. *Appl. Catal. B Environ.* **2003**, *46*, 121–132. [[CrossRef](#)]
22. Boix, A.V.; Miró, E.E.; Lombardo, E.A.; Mariscal, R.; Fierro, J.L.G. Binder Effect upon the Catalytic Behavior of PtCoZSM5 Washcoated on Cordierite Monoliths. *Appl. Catal. A Gen.* **2004**, *276*, 197–205. [[CrossRef](#)]
23. Boix, A.V.; Lombardo, E.A.; Miró, E.E. Effect of the Pt/Co Ratio upon the Catalytic Behavior of PtCoFerrierite Washcoated on Cordierite Monoliths. *Catal. Today* **2005**, *107–108*, 330–337. [[CrossRef](#)]
24. Boix, A.V.; Aspromonte, S.G.; Miró, E.E. Deactivation Studies of the SCR of NO_x with Hydrocarbons on Co-Mordenite Monolithic Catalysts. *Appl. Catal. A Gen.* **2008**, *341*, 26–34. [[CrossRef](#)]
25. Cortés-Reyes, M.; Herrera, C.; Larrubia, M.Á.; Alemany, L.J. Advance in the Scaling up of a Hybrid Catalyst for NSR-SCR Coupled Systems under H₂O + CO₂ Atmosphere. *Catal. Today* **2020**, *356*, 292–300. [[CrossRef](#)]
26. Azzoni, M.E.; Franchi, F.S.; Usberti, N.; Nasello, N.D.; Castoldi, L.; Nova, I.; Tronconi, E. Dual-Layer AdSCR Monolith Catalysts: A New Solution for NO_x Emissions Control in Cold Start Applications. *Appl. Catal. B Environ.* **2022**, *315*, 121544. [[CrossRef](#)]
27. Serra, R.M.; Aspromonte, S.G.; Miró, E.E.; Boix, A.V. Hydrocarbon Adsorption and NO_x-SCR on (Cs,Co)Mordenite. *Appl. Catal. B Environ.* **2015**, *166–167*, 592–602. [[CrossRef](#)]
28. Lónyi, F.; Solt, H.E.; Pászti, Z.; Valyon, J. Mechanism of NO-SCR by Methane over Co,H-ZSM-5 and Co,H-Mordenite Catalysts. *Appl. Catal. B Environ.* **2014**, *150–151*, 218–229. [[CrossRef](#)]
29. Boix, A.; Fierro, J.L.G. X-Ray Photoelectron Spectroscopy Analysis of Platinum- and/or Cobalt-Loaded Zeolites Relevant for Selective Catalytic Reduction of NO_x. *Surf. Interface Anal.* **1999**, *27*, 1107–1113. [[CrossRef](#)]
30. Zsoldos, Z.; Vass, G.; Lu, G.; Guzzi, L. XPS Study on the Effects of Treatments on Pt²⁺ and Co²⁺ Exchanged into NaY Zeolite. *Appl. Surf. Sci.* **1994**, *78*, 467–475. [[CrossRef](#)]
31. Dutta, N.C.; Iwasaki, T.; Ebina, T.; Hayashi, H. A Combined X-Ray Photoelectron and Auger Electron Spectroscopic Study of Cesium in Variable-Charge Montmorillonites. *J. Colloid Interface Sci.* **1999**, *216*, 161–166. [[CrossRef](#)] [[PubMed](#)]
32. Tang, C.W.; Wang, C.B.; Chien, S.H. Characterization of Cobalt Oxides Studied by FT-IR, Raman, TPR and TG-MS. *Thermochim. Acta* **2008**, *473*, 68–73. [[CrossRef](#)]
33. Gómez, L.E.; Múnera, J.F.; Sollier, B.M.; Miró, E.E.; Boix, A.V. Raman in Situ Characterization of the Species Present in Co/CeO₂ and Co/ZrO₂ Catalysts during the COPrOx Reaction. *Int. J. Hydrogen Energy* **2016**, *41*, 4993–5002. [[CrossRef](#)]
34. Boix, A.; Miró, E.E.; Lombardo, E.A.; Bañares, M.A.; Mariscal, R.; Fierro, J.L.G. The Nature of Cobalt Species in Co and PtCoZSM5 Used for the SCR of NO_x with CH₄. *J. Catal.* **2003**, *217*, 186–194. [[CrossRef](#)]
35. Ohtsuka, H.; Tabata, T.; Okada, O.; Sabatino, L.M.F.; Bellussi, G. A Study on the Roles of Cobalt Species in NO_x Reduction by Propane on Co-Beta. *Catal. Today* **1998**, *42*, 45–50. [[CrossRef](#)]
36. Band, A.; Abu-Yaron, A.; Livneh, T.; Cohen, H.; Feldman, Y.; Shimon, L.; Popovitz-Biro, R.; Lyahovitskaya, V.; Tenne, R. Characterization of Oxides of Cesium. *J. Phys. Chem. B* **2004**, *108*, 12360–12367. [[CrossRef](#)]
37. Kraus, M.; Trommler, U.; Holzer, F.; Kopinke, F.-D.; Roland, U. Competing Adsorption of Toluene and Water on Various Zeolites. *Chem. Eng. J.* **2018**, *351*, 356–363. [[CrossRef](#)]
38. Hussein, M.S.; Ahmed, M.J. Fixed Bed and Batch Adsorption of Benzene and Toluene from Aromatic Hydrocarbons on 5A Molecular Sieve Zeolite. *Mater. Chem. Phys.* **2016**, *181*, 512–517. [[CrossRef](#)]
39. Zhu, J.; Zhang, P.; Wang, Y.; Wen, K.; Su, X.; Zhu, R.; He, H.; Xi, Y. Effect of Acid Activation of Palygorskite on Their Toluene Adsorption Behaviors. *Appl. Clay Sci.* **2018**, *159*, 60–67. [[CrossRef](#)]
40. Kustov, L.; Golubeva, V.; Korableva, A.; Anischenko, O.; Yegorushina, N.; Kapustin, G. Alkaline-Modified ZSM-5 Zeolite to Control Hydrocarbon Cold-Start Emission. *Microporous Mesoporous Mater.* **2018**, *260*, 54–58. [[CrossRef](#)]
41. Takamitsu, Y.; Ariga, K.; Yoshida, S.; Ogawa, H.; Sano, T. Adsorption of Toluene on Alkali Metal Ion-Exchanged ZSM-5 and β-Zeolites under Humid Conditions. *Bull. Chem. Soc. Jpn.* **2012**, *85*, 869–876. [[CrossRef](#)]
42. William Corning Inc. Modified Large Pore Zeolites for Trapping Alkenes. Patent EP 0639400 A1, 4 April 2016.
43. Martins, L.; Holderich, W.; Cardoso, D. Methylammonium-FAU Zeolite: Investigation of the Basic Sites in Base Catalyzed Reactions and Its Performance. *J. Catal.* **2008**, *258*, 14–24. [[CrossRef](#)]
44. Oh, H.; Beum, H.T.; Yoon, Y.-S.; Kim, J.; Han, Y.; Kim, J.; Lee, I.-B.; Lee, S.-Y.; Han, S.S. Experiment and Modeling of Adsorption of CO from Blast Furnace Gas onto CuCl/Boehmite. *Ind. Eng. Chem. Res.* **2020**, *59*, 12176–12185. [[CrossRef](#)]
45. Czaplewski, K.F.; Reitz, T.L.; Kim, Y.J.; Snurr, R.Q. One-Dimensional Zeolites as Hydrocarbon Traps. *Microporous Mesoporous Mater.* **2002**, *56*, 55–64. [[CrossRef](#)]
46. Wesson, P.J.; Snurr, R.Q. Modified Temperature Programmed Desorption Evaluation of Hydrocarbon Trapping by CsMOR Zeolite under Cold Start Conditions. *Microporous Mesoporous Mater.* **2009**, *125*, 35–38. [[CrossRef](#)]

47. Westermann, A.; Azambre, B. Impact of the Zeolite Structure and Acidity on the Adsorption of Unburnt Hydrocarbons Relevant to Cold Start Conditions. *J. Phys. Chem. C* **2016**, *120*, 25903–25914. [[CrossRef](#)]
48. Zhao, W.; Ruan, S.; Qian, S.; Feng, B.; Ao, C.; Wang, L.; Liu, F.; Zhang, L. Abatement of n -Butane by Catalytic Combustion over Co-ZSM-5 Catalysts. *Energy Fuels* **2020**, *34*, 12880–12890. [[CrossRef](#)]
49. Zhang, W.; Zhou, Y.; Shamzhy, M.; Molitorisová, S.; Opanasenko, M.; Giroir-Fendler, A. Total Oxidation of Toluene and Propane over Supported Co₃O₄ Catalysts: Effect of Structure/Acidity of MWW Zeolite and Cobalt Loading. *ACS Appl. Mater. Interfaces* **2021**, *13*, 15143–15158. [[CrossRef](#)]
50. Pietrzyk, P.; Dujardin, C.; Góra-Marek, K.; Granger, P.; Sojka, Z. Spectroscopic IR, EPR, and OperandoDRIFT Insights into Surface Reaction Pathways of Selective Reduction of NO by Propene over the Co-BEAzeolite. *Phys. Chem. Chem. Phys.* **2012**, *14*, 2203–2215. [[CrossRef](#)]
51. Shilina, M.I.; Rostovshchikova, T.N.; Nikolaev, S.A.; Udalova, O.V. Polynuclear Co-Oxo Cations in the Catalytic Oxidation of CO on Co-Modified ZSM-5 Zeolites. *Mater. Chem. Phys.* **2019**, *223*, 287–298. [[CrossRef](#)]
52. Lim, J.B.; Shin, J.; Ahn, N.H.; Heo, I.; Hong, S.B. Selective Catalytic Reduction of NO with CH₄ over Cobalt-Exchanged Cage-Based, Small-Pore Zeolites with Different Framework Structures. *Appl. Catal. B Environ.* **2020**, *267*, 118710. [[CrossRef](#)]
53. Aspromonte, S.G.; Boix, A.V. The Nature of Cobalt Species in Co-Zeolites Used for the Selective Catalytic Reduction of NO_x with Hydrocarbons. In *Cobalt: Occurrence, Uses and Properties*; Kobayashi, Y., Suzuki, H., Eds.; Nova Science Publishers, Inc.: Hauppauge, NY, USA, 2013; p. 135. ISBN 978-1-62808-278-4.
54. Wu, D.; Zhang, H. Mechanical Stability of Monolithic Catalysts: Scattering of Washcoat Adhesion and Failure Mechanism of Active Material. *Ind. Eng. Chem. Res.* **2013**, *52*, 14713–14721. [[CrossRef](#)]

Disclaimer/Publisher's Note: The statements, opinions and data contained in all publications are solely those of the individual author(s) and contributor(s) and not of MDPI and/or the editor(s). MDPI and/or the editor(s) disclaim responsibility for any injury to people or property resulting from any ideas, methods, instructions or products referred to in the content.